JACS
JOURNAL OF THE AMERICAN CHEMICAL SOCIETY
Article
pubs.acs.org/JACS

A pH-Sensitive, Colorful, Lanthanide-Chelating Paramagnetic NMR Probe

Wei-Min Liu, Peter H. J. Keizers, Mathias A. S. Hass, Anneloes Blok, Monika Timmer, Alexi J. C. Sarris, Mark Overhand, and Marcellus Ubbink*

Gorlaeus Laboratories, Leiden Institute of Chemistry, Leiden University, 2300 RA Leiden, The Netherlands

Supporting Information

ABSTRACT: Paramagnetic lanthanides ions are broadly used in NMR spectroscopy. The effects of unpaired electrons on NMR spectral parameters provide a powerful tool for the characterization of macromolecular structures and dynamics. Here, a new lanthanide-chelating NMR probe, Caged Lanthanide NMR Probe-7 (CLaNP-7), is presented. It can be attached to protein surfaces via two disulfide bridges, yielding a probe that is rigid relative to the protein backbone. CLaNP-7 extends the application range of available probes. It has a yellow color, which is helpful for sample preparation. Its effects are comparable to those of CLaNP-5, but its charge is two units lower (+1) than that of CLaNP-5 (+3), reducing the change in surface potential after probe attachment. It also has a different magnetic susceptibility tensor, so by using both tags, two sets of structural restraints can be obtained per engineered cysteine pair. Moreover, it was found that the orientation of the magnetic susceptibility tensor is pH dependent ($pK_a \approx 7$) when a histidine residue is located in the neighborhood of the probe attachment site. The results show that the His imidazole group interacts with the CLaNP-7 tag. It is proposed that the histidine residue forms a hydrogen bond to a water/hydroxyl molecule that occupies the ninth coordination position on the lanthanide, thus breaking the two-fold symmetry of the CLaNP tag in a pH-dependent way.

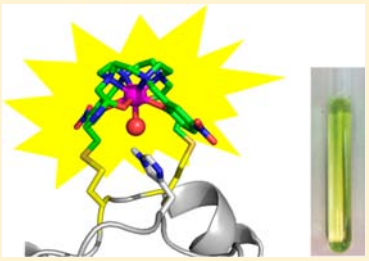

INTRODUCTION

In recent years, paramagnetic probes have been used broadly in nuclear magnetic resonance (NMR) spectroscopy. The effects of unpaired electrons on NMR spectral parameters, such as pseudocontact shifts (PCSs), residual dipolar couplings (RDCs), and nuclear relaxation enhancements, have been recognized as powerful tools for the characterization of macromolecular structures and their dynamics and interactions.[1−8] Among the paramagnetic effects, PCSs yield valuable long-range distance and orientation information and RDCs are distance-independent, providing information on the whole protein, making them powerful restraints to refine protein structures and determine protein orientations in complexes.[9]

To yield unambiguous restraints, the paramagnetic center must be site-specifically and rigidly attached to the protein. For Ca^{2+}- or Mg^{2+}-containing metalloproteins, lanthanide ions can substitute the natural metal,[10−12] but most proteins are devoid of these metal binding sites. Therefore, several methods have been developed to introduce artificial paramagnetic metals into protein. For instance, metal binding peptide tags were designed that can be engineered genetically at the N or C terminus or into a loop region of a protein.[13−17] Other strategies use synthetic organic thio-functional tags, which can be introduced via cysteine mutations.[3,18,19]

1,4,7,10-Tetraazacyclododecane-1,4,7,10-tetraacetic acid (DOTA) is a typical chelator for lanthanide ions. The coordination of DOTA to lanthanide ions results in two stable diastereomers, a square antiprism (SA) and a twisted square antiprism (TSA).[20−23] Each diastereomer relates to one of two possible configurations of the macrocycle rings ($\lambda\lambda\lambda\lambda$ and $\delta\delta\delta\delta$) and one of two orientations of the chelate arms (Δ and Λ). The enantiomers $\Delta\lambda\lambda\lambda\lambda$ and $\Lambda\delta\delta\delta\delta$ belong to the SA structures, whereas the pair of $\Lambda\lambda\lambda\lambda$ and $\Delta\delta\delta\delta$ forms the TSA conformation. In previous studies, we have developed paramagnetic lanthanide probes based on cyclen.[24−26] The probes are attached to target proteins via two disulfide bridges, which strongly reduces the mobility.[24] In the most recent version, two chelating pyridine-*N*-oxide arms force the probe to exist into one diastereomer, the SA form, in the solution state.[25,27] This results in singular NMR resonances and one magnetic susceptibility tensor. This probe, named Caged Lanthanide NMR Probe-5 (CLaNP-5, Figure 1), showed the largest PCSs and RDCs described so far.[25] A drawback is the total charge of the probe, which is 3+ after chelation with a lanthanide ion. When CLaNP-5 is linked to a protein surface, the extra charge changes the electrostatic potential, which may affect molecular interactions with ligands and proteins. In the current study, a new tag is described (CLaNP-7, Figure 1) that has a reduced net charge while maintaining conformational rigidity. Ln-CLaNP-7 complexes have different magnetic susceptibilities than those of CLaNP-5 and its endogenous color allows for easy detection of tagged protein. Furthermore, we show that CLaNP-7 can interact with a nearby histidine residue, causing a pH dependence of the magnetic susceptibility tensor (χ-tensor). It was shown that two sets of distance

Received: August 13, 2012
Published: September 21, 2012

   dx.doi.org/10.1021/ja307824e | J. Am. Chem. Soc. 2012, 134, 17306−17313

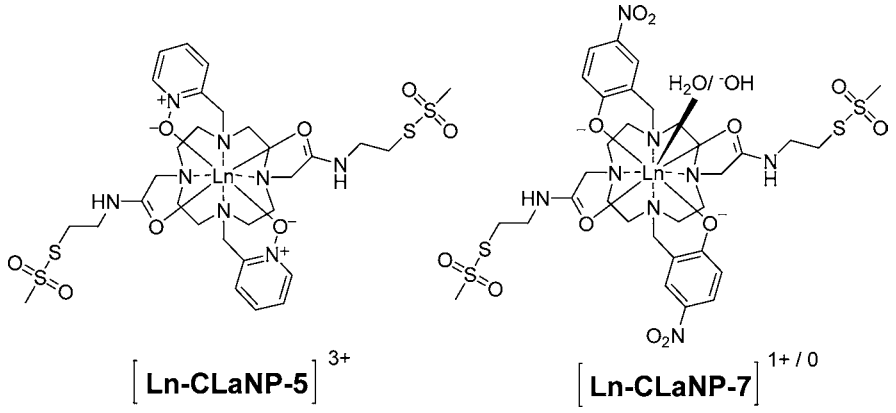

Figure 1. Structures of Ln-CLaNP-5[24] and Ln-CLaNP-7.

Scheme 1[a]

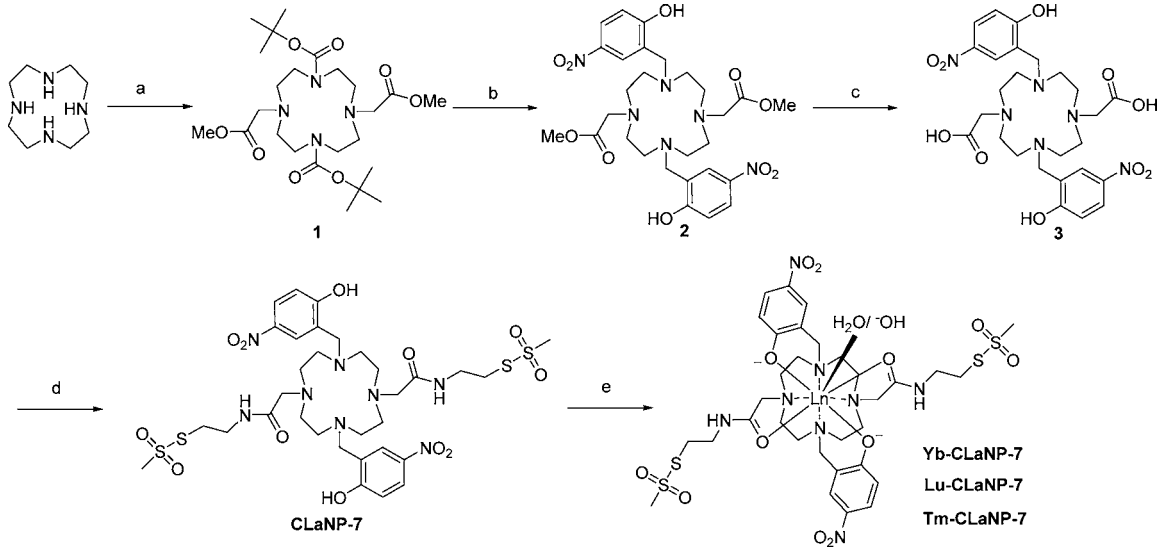

[a]Reagents and conditions: (a) (i) BocOSu, $CHCl_3$, rt, 36 h; (ii) methyl bromoacetate, K_2CO_3, rt, 12 h. (b) (i) TFA, DCM, rt, 4 h; (ii) 2-hydroxy-5-nitrobenzyl bromide, K_2CO_3, ACN, 80 °C, 12 h. (c) NaOH, 1,4-dioxane, rt, 4 h. (d) Aminoethyl-MTS, NHS, EDC, DMF, rt, overnight. (e) $Ln(OAc)_3$, DMF, rt, 4 h, quant.

restraints can be obtained, simply by changing the pH. A model for the pH-dependent interaction is proposed.

RESULTS

Synthesis of Caged Lanthanide NMR Probe-7. In 2004, Sherry's group published a study on a magnetic resonance imaging (MRI) contrast agent based on the cyclen scaffold and carrying a *p*-nitrophenol ligating group.[28] The crystal structure of the MRI contrast agent indicated that the phenol is deprotonated and a water molecule sits above the plane of the oxygen atoms. In order to design a rigid cyclen based probe with a reduction of net positive charge, the pyridine-*N*-oxide arms used for CLaNP-5 were replaced with *p*-nitrophenol arms (Figure 1). The *p*-nitro groups enhance the acidity of the phenolic protons and upon binding the lanthanide, the phenol groups will be deprotonated. As the lanthanide has a charge of +3, the net charge of the entire complex will be +1, unless a hydroxyl ion rather than a water molecule can coordinate, in which case the overall charge is zero (see below). The two *p*-nitrophenol groups provide C_2 symmetry, and it was anticipated that the two six-member ring chelating systems (Figure 1) provide sufficient rigidity and thus lead to one preferred tetraazacyclododecane ring conformation.[27] The yellow color associated with *p*-nitrophenolate groups is convenient for the purification of tagged proteins.

The synthesis of CLaNP-7 is shown in Scheme 1. Commercially available cyclen was converted into **1** in 83% yield over two steps, in which two opposing amines were temporarily protected with *tert*-butoxycarbonyl (Boc) groups and the other two amines subsequently functionalized by reaction with methyl bromoacetate.[29] Compound **1** was deprotected by trifluoroacetic acid (TFA) and reacted with 2-hydroxy-5-nitrobenzyl bromide at 80 °C to obtain **2**.[28,30] Removal of the methyl ester group in the presence of base in 1,4-dioxane as solvent yielded **3**.[31] Condensation of **3** with excess (2-aminoethyl)methanethiosulfonate in presence of 1-ethyl-3-(3-dimethylaminopropyl)carbodiimide (EDC) and *N*-hydroxysuccinimide (NHS) yielded CLaNP-7 in 40% yield. The Yb-CLaNP-7, Tm-CLaNP-7, and Lu-CLaNP-7 complexes were obtained by chelating with the corresponding lanthanide acetate salts in *N*,*N*-dimethylformamide (DMF). After chelation, the wavelength of the maximum absorbance shifted from 310 to 390 nm, and the tag obtained a more intense yellow color (Figure 2A).

dx.doi.org/10.1021/ja307824e | J. Am. Chem. Soc. 2012, 134, 17306−17313

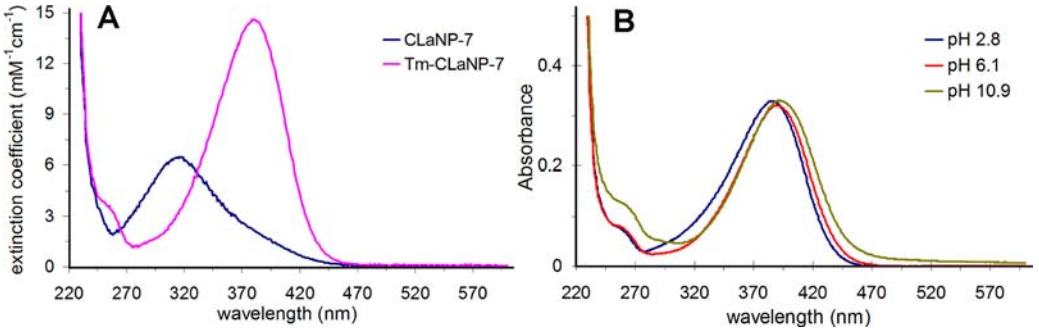

Figure 2. Electronic absorption spectra of CLaNP-7. (A) The absorbance spectra expressed as extinction coefficients are plotted for CLaNP-7 and Tm-CLaNP-7. (B) Lu-CLaNP-7 at different pH values.

Probe Attachment and $\Delta\chi$-Tensors Calculation. The Zn^{2+} form of ^{15}N-enriched E51C/E54C pseudoazurin (Paz) was reduced with dithiothreitol (DTT), washed, and directly incubated with Ln-CLaNP-7 for 16 h at 4 °C. The tagged protein was purified using a Superdex 75 column (GE Healthcare). The mass of the resulting ^{15}N-Paz Yb-CLaNP-7 (14 503 ± 2 Da) agreed with the expected mass of 14 503 Da, assuming 98% ^{15}N enrichment. In the [^{15}N,^{1}H]-HSQC spectra, there were no significant differences between untagged and Lu-CLaNP-7 tagged spectra, except for a few residues close to the attachment site, enabling the resonance assignments to be made by comparison with previous spectra.[32] Large shifts of resonances were observed when the protein was tagged with either Yb-CLaNP-7 or Tm-CLaNP-7 (Figure 3).

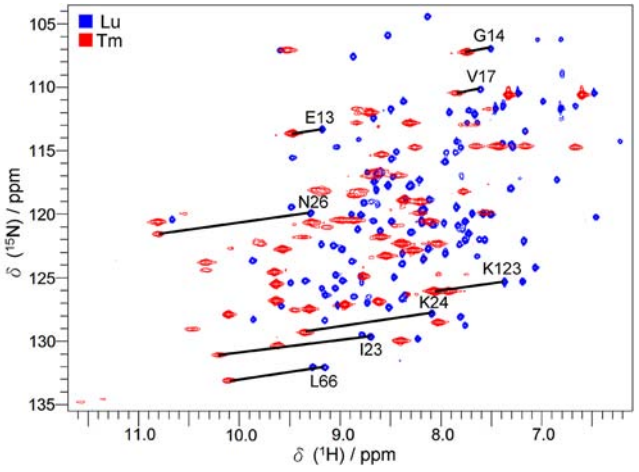

Figure 3. Overlay of [^{15}N,^{1}H]-HSQC spectra of Paz E51C/E54C attached to Lu-CLaNP-7 (blue) and Tm-CLaNP-7 (red). Several PCSs are indicated with solid lines.

The difference in resonance frequency between the paramagnetic and the diamagnetic samples was defined as the PCS. The presence of large, single PCSs indicates the tag to be attached rigidly and to exist in one dominant conformation, which is expected to be the SA isomer due to the six-member chelating system (but see Discussion section).[27]

For estimation of the anisotropic component of the magnetic susceptibility tensor ($\Delta\chi$-tensors), an initial metal position was fixed according to a previously reported protocol.[25] An initial set of PCSs was used to determine the $\Delta\chi$-tensor, with which more PCSs were predicted. In an iterative way, the $\Delta\chi$-tensor and metal position were refined and additional resonances were assigned. The $\Delta\chi$-tensor values for Tm- and Yb-CLaNP-7, along with those of CLaNP-5 are reported in Table 1 and the back-calculated PCSs are plotted versus the observed PCSs in Figures 4A and S1, respectively. The values of $\Delta\chi_{ax}$ and $\Delta\chi_{rh}$ of CLaNP-7 are similar to those of CLaNP-5 for Tm, but not for Yb. The $\Delta\chi$-tensor of Yb-ClaNP-7 is much more rhombic. A possible explanation could be the presence of a ninth ligand, a water molecule or hydroxyl ion. This possibility is discussed in more detail in the next section. Tm-CLaNP-7 causes significant alignment of Paz at 600 MHz (14.1 T), allowing RDCs up to 20 Hz to be observed. The observed RDCs were used to optimize the HN positions of Paz and the $\Delta\chi$-tensor derived from PCS was used to back-calculate the RDCs on the basis of this structure, yielding a good agreement (Figure 4B). The large RDCs indicate a low mobility of CLaNP-7 relative to the protein backbone.

pH Dependence of CLaNP-7. In order to test CLaNP-7 on a second protein, yeast cytochrome *c* (Cyt *c*) N56C/L58C was tagged with CLaNP-7 coordinated to Yb and Lu. In the diamagnetic spectrum (Lu-CLaNP-7) only single peaks were observed. However, at pH 7, the Cyt *c* tagged with Yb-CLaNP-7 showed two sets of peaks for most residues. The relative intensity and sometimes the sign as well changed with pH (Figures 5 and S2). From the PCSs obtained at pH 6 and 8, the $\Delta\chi$-tensors were determined. A comparison of the PCSs shows that they differ significantly (Figure S3). The sizes of the axial and rhombic components are similar at both pH values and somewhat larger than for Paz E51C/E54C (Table 1 and Figure S4). The major difference between pH 6 and 8 is the orientation of the tensors (Figure 6A). The structurally highly similar tag Ln-CLaNP-5 shows a single set of resonances when attached to the same double Cys mutant of Cyt *c* (Figure S5).[33] Also for CLaNP-7 attached to Paz E51C/E54C no pH dependence of the PCS was observed, so the observed effect is specific for CLaNP-7 attached to Cyt *c* N56C/L58C.

Protonation of the phenol moiety of CLaNP-7 as an explanation for the pH dependence was ruled out by the electronic absorption spectrum. Protonation of the phenol shifts the absorbance maximum from 390 to 310 nm.[34] From Figure 2A, it is clear that in free CLaNP-7 purified by HPLC the phenol rings are protonated, but upon coordination to Tm or Lu they are deprotonated at pH values between 3 and 11 (Figure 2B). In general, there is a water coordinated to the DOTA-like lanthanide ions complex in solution state.[35] The factors that affect water coordination are mainly the charge density of the lanthanide ion and the steric strain at the water binding site.[36−38] The substitution of the pyridine-*N*-oxide rings in CLaNP-5 with *p*-nitrophenol rings in CLaNP-7 lowers the charge of the coordinated oxygen of the ligand, which

dx.doi.org/10.1021/ja307824e | J. Am. Chem. Soc. 2012, 134, 17306−17313

Table 1. PCSs-Based $\Delta\chi$-Tensors of CLaNP-5[25] and CLaNP-7[a]

protein	probe	Ln	$\Delta\chi_{ax}$[b]	$\Delta\chi_{rh}$[b]	restraints	Q[c]
Paz E51C/E54C	CLaNP-5	Tm	55.5 ± 0.8	10 ± 1	89	0.03
		Yb	9.4 ± 0.2	1.9 ± 0.4	93	0.04
	CLaNP-7	Tm	41.4 ± 0.6	9.6 ± 0.8	94	0.04
		Yb	4.2 ± 0.1	5.6 ± 0.4	93	0.06
Cyt *c* N56/L58C	CLaNP-7 (pH 6)	Yb	6.3 ± 0.4	8.0 ± 0.3	70	0.03
	CLaNP-7 (pH 8)	Yb	5.5 ± 0.9	9.6 ± 0.3	60	0.06
Cyt *c* N56C/L58C/H39A	CLaNP-7 (pH 6.3)	Yb	5.5 ± 0.2	6.5 ± 0.1	70	0.04
	CLaNP-7 (pH 7.8)	Yb	5.5 ± 0.1	6.1 ± 0.1	62	0.04

[a]The unit of axial and rhombic components $\Delta\chi_{ax}$ and $\Delta\chi_{rh}$ is 10^{-32} m^3. [b]The error is calculated by a jackknife procedure, randomly removing 20% of the data and repeating the $\Delta\chi$-tensor fit 100 times. [c]Q is defined in the Experimental Section (eq 2).

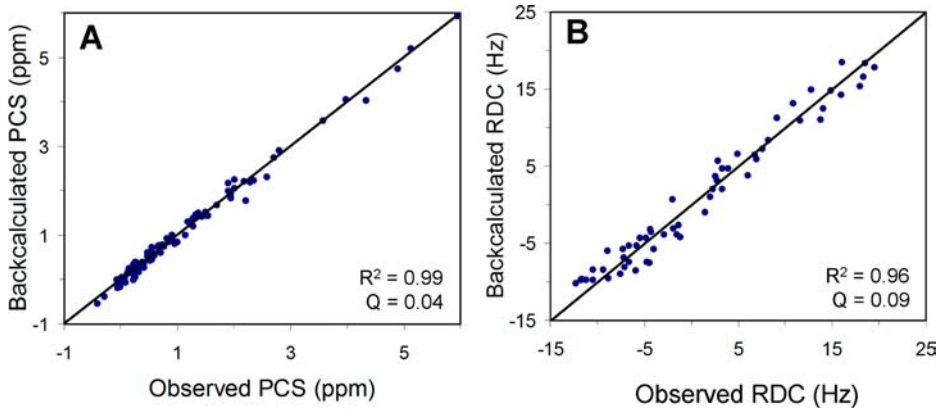

Figure 4. Experimentally observed amide proton PCSs and RDCs of Paz E51C/E54C Tm-CLaNP-7 plotted against the back-calculated PCSs (A, Q = 0.04) and RDCs (B, Q = 0.09), both based on the PCS derived $\Delta\chi$-tensor. The NMR spectra were recorded at 14.1 T (600 MHz). The solid line represents a perfect match.

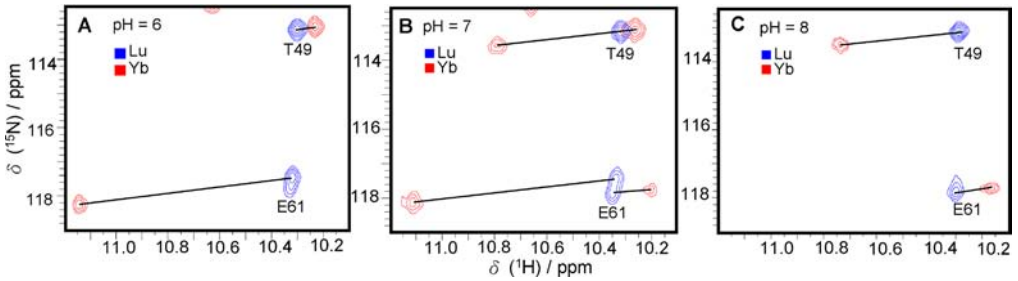

Figure 5. pH dependence of CLaNP-7. Detail of [^{15}N,^{1}H]-HSQC spectra of Cyt *c* N56C/L58C attached to Lu-CLaNP-7 (blue) and Yb-CLaNP-7 (red) at pH 6.0 (A), 7.0 (B), and 8.0 (C).

results in a larger space for a ninth coordination.[27,28] Thus, it is likely that a water molecule or hydroxyl ion can be coordinated to the lanthanide.

In Cyt *c* N56C/L58C, the Cys residues are located in a short β-strand and there is a histidine residue, His 39, in the neighboring strand, close to the tag attachment site. Fitting of the PCSs placed the lanthanide close to His 39, and its imidazole ring can be rotated to be at hydrogen bond distance of a water molecule at the ninth coordination position (Figure 6B). Therefore, we propose that the observed pH dependence of the $\Delta\chi$-tensor is caused by the imidazole of His 39.

In order to test this hypothesis, the His residue in Cyt *c* N56C/L58C was mutated to alanine and this variant was labeled with Ln-CLaNP-7. The pH dependence of the $\Delta\chi$-tensor is no longer observed in the absence of the imidazole ring. The [^{15}N,^{1}H]-HSQC spectra shows single peaks at several pH values (Figure S6A) and the PCS and the $\Delta\chi$-tensors are the same at low and high pH (Table 1 and Figure S7). The peaks only exhibit small shifts due to the normal pH dependence of the protein and those shifts are identical in paramagnetic and diamagnetic samples (Figure S6B). These observations support the proposal that His 39 influences the $\Delta\chi$-tensor in a pH-dependent manner.

We wondered whether it was possible to introduce the pH dependence of the tensor by positioning the probe close to a His residue on a protein surface. For this purpose we returned to Paz, which is a β-sheet protein. His 6 is located on a long β-strand. In the neighboring strand two Cys residues were engineered, mutant I34C/V36C. Using the published protocol for modeling of the CLaNP lanthanide position,[25] it was predicted that the imidazole ring of His 6 would be sufficiently close to form a H-bond to a possible H_2O/OH at the ninth

dx.doi.org/10.1021/ja307824e | J. Am. Chem. Soc. 2012, 134, 17306−17313

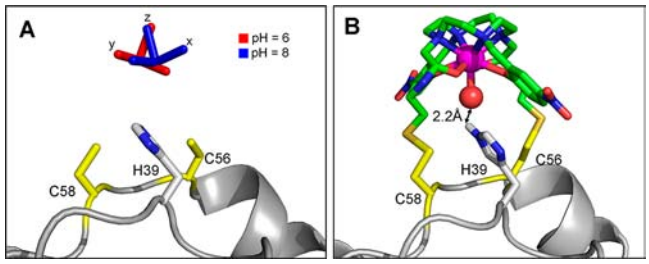

Figure 6. PCS-based positions of the tensor relative to the Cyt *c* structure with PDB entry code 1YCC.[39] The Cys residues at positions 56 and 58 were modeled. (A) The principal axes of the $\Delta\chi$-tensor of Yb-CLaNP-7 are shown as red (pH 6) and blue sticks (pH 8). (B) Model of CLaNP-7 attached to Cyt *c* N56C/L58C. The position of the Yb (magenta) is derived from a fit to the PCS data. The red sphere shows the H_2O/OH at the ninth coordination position. The protein main chain is shown in gray. The Cys (N56C/L58C) and the His 39 side chains are shown in yellow and CPK colors, respectively. The carbon atoms from CLaNP-7 are shown in green, nitrogen atoms in blue, oxygen atoms in red and sulfur atoms in yellow. The distance between the $H^{\epsilon 2}$ of His 39 and the ligating oxygen atom is 2.2 Å.

coordination position (Figure S8). The HSQC spectra clearly show two peaks for most resonances in this Paz variant labeled with Yb-CLaNP-7 and the intensity of these peaks indeed varies with pH, analogous to what was observed for Cyt *c* N56C/L58C (Figure 7). Note that Paz E51C/E54C labeled with

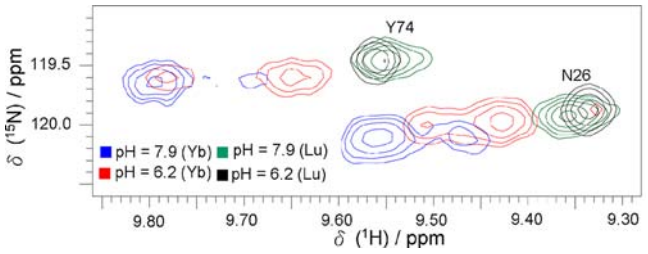

Figure 7. Detail of [^{15}N,^{1}H]-HSQC spectra of Ln-CLaNP-7 tagged ^{15}N-labeled Paz I34C/V36C. The spectra were recorded at pH 6.2 (black, Lu; red, Yb) and pH 7.9 (green, Lu; blue, Yb).

CLaNP-7 did not show pH dependence. These results indicate that the pH dependence of the $\Delta\chi$-tensor can be introduced when the probe is positioned on a β-sheet, next to a histidine residue. The pH dependence of CLaNP-7 may be used to obtain two independent sets of PCSs or RDCs from a single probe.

DISCUSSION

Proposed Mechanism for CLaNP-7 pH Dependence. Based on the $\Delta\chi$-tensor, the position of the Yb-CLaNP-7 linked to Cyt *c* N56C/L58C is the same within error at pH 6 and 8. However, the orientations of the tensors are different (Figure 6A). The two sets of peaks in the HSQC spectra of Yb-labeled protein indicate that these orientations are a consequence of two orientations/conformations of the probe that are in slow exchange on the NMR chemical shift time scale. In contrast to what is expected for a simple pH titration in which the two sets of peaks would correspond to a protonated and deprotonated form, here both sets of peaks remain (weakly) visible, even at the highest and lowest pH values applied. Furthermore, not only do the relative intensities of the pairs of peaks change with pH, the PCSs of both states also exhibit some pH dependence (Figure S9).

In order to explain these observations, a four-state model is invoked (Figure 8). The model hypothesizes that the two-fold symmetry of the probe is broken by the interaction between the imidazole of the nearby histidine and the proposed H_2O/OH coordinated to the Yb. Consequently, the two SA enantiomers ($\Delta\lambda\lambda\lambda\lambda$ and $\Lambda\delta\delta\delta\delta$) no longer yield identical PCS and now cause double peaks, because cyclen ring flips are normally slow.[40,41] Protonation/deprotonation of the imidazole shifts the equilibrium between these two states. It also causes the pH dependence of the PCSs of both states (Figure S9). The intensity ratio (I_b/I_a) of the pairs of peaks can be described on the basis of this model by eq 1:

$$\frac{I_b}{I_a} = K\frac{[1 + 10^{(pH-pK_{a2})}]}{[1 + 10^{(pH-pK_{a1})}]} \quad (1)$$

where I_a and I_b are the peaks intensity of the two sets of peaks and I_b is most intense at high pH, K is the equilibrium constant, and pK_{a1} and pK_{a2} are the proton association constants. Fitting the observed intensity ratio of the peaks for Cyt *c* N56C/L58C to eq 1 yields the curve given in Figure 8B. The equilibrium changes from $K = 0.52$ to $K' = 3.36$, where $K' = K(K_{a1}/K_{a2})$, so state III becomes the dominant conformation when going from high to low pH. For Paz I34C/V36C the effect is also clearly present, although the shift in the equilibrium is smaller (Figure 8B).

Comparison with CLaNP-5. Tm-CLaNP-5 and Tm-CLaNP-7 were attached to Paz E51C/E54C, and both caused large PCSs and RDCs, but these shifts and couplings differ in size and sometimes sign as well (Figure S10). The position of the metal, as well as the size and orientation of the $\Delta\chi$-tensor were obtained by fitting to the PCS data. The PCS histograms have an overall similar appearance for both tags because PCS is dominated by the distance between the nucleus and the metal. However, detailed inspection shows clear differences that reflect the somewhat smaller size and changed orientation of the CLaNP-7 $\Delta\chi$-tensor. Also the positions of the Ln ions are different by 3.4 Å (Figure 9C). The RDC histograms show many more differences (Figure S10B), because RDC is solely dependent on the H−N bond vector orientation in the $\Delta\chi$-tensor frame. The RDCs range from −15 to +20 Hz for Tm-CLaNP-7 and from −20 to +30 Hz for Tm-CLaNP-5 at 14.1 T (600 MHz). The observed PCSs and RDCs of CLaNP-7 were plotted versus the observed PCSs and RDCs of CLaNP-5 (Figure 9) and showed poor agreement between CLaNP-5 and CLaNP-7. It is concluded that the two probes cause sufficiently different effects to yield complementary structural restraints from a single attachment site.

CONCLUSION

CLaNP-7 is a new two-armed lanthanide chelating protein probe that provides large PCSs and RDCs. CLaNP-7 and CLaNP-5 have different magnetic susceptibility tensors, providing a convenient way to obtain different paramagnetic effects from the same target protein with a single set of engineered Cys residues. In addition, the lower net charge of CLaNP-7 will be beneficial in protein−protein interaction studies. CLaNP-7 has a bright yellow color simplifying the sample handling, and importantly, it is the first example of a pH-sensitive paramagnetic probe offering a unique opportunity to tune paramagnetic effects.

dx.doi.org/10.1021/ja307824e | J. Am. Chem. Soc. 2012, 134, 17306−17313

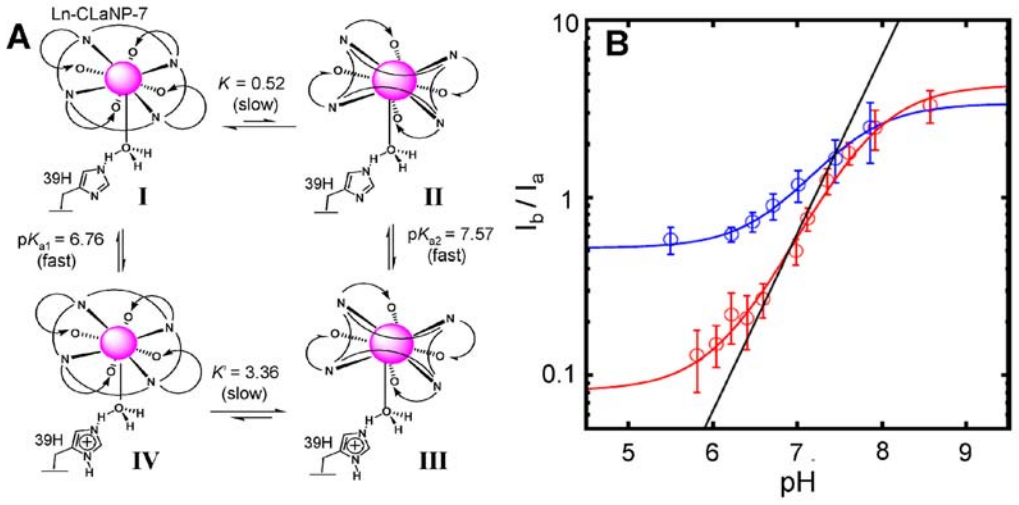

Figure 8. Proposed model to describe pH dependence of CLaNP-7. (A) The flip between two SA forms ($\Delta\lambda\lambda\lambda\lambda$ and $\Lambda\delta\delta\delta\delta$) are schematically represented by a change in the cyclen ring (lines connecting the N atoms) and the ligand arms (round arrows). The values were obtained from a fit to the I_b/I_a ratios of Cyt *c* N56C/L58C at multiple pH values (eq 1). (B) Intensity ratios as a function of pH. The averaged intensity ratios for pairs of resonances in Cyt *c* N56C/L58C (red) and Paz I34C/V36C (blue) are plotted as a function of pH. The solid lines represent fits to the model described in the text (eq 1). The intensity ratios are averaged from 13 residues for Cyt *c* and 10 residues for Paz and the error bars are the standard deviation. The black line represents a standard deprotonation curve.

EXPERIMENTAL SECTION

General. $Ln(OAc)_3$, cyclen, 2-(aminoethyl)methanethiosulfonate hydrobromide, 2-hydroxy-5-nitrobenzyl bromide, and all other chemicals were used as purchased without further purification. Thin-layer chromatography analysis was conducted on a DC-alufolien instrument (Merck, Kieselgel60, F254) with detection by UV absorption (254 nm). Flash chromatography was performed on Screening Devices silica gel 60 (0.04−0.063 mm). A Biocad Vision HPLC instrument (PerSeptive Biosystems, Inc.) and an Akta Basic FPLC instrument (GE Healthcare Inc.) were used for purifications. Analytical, semipreparative, and preparative reversed-phase C18 columns were obtained from Phenomenex (Torrance, CA). Superdex 75, CM sepharose, and HiTrap SP columns were obtained from GE Healthcare. NMR spectra were recorded on a Bruker AV-400 (400/100 MHz) and Bruker Avance-III 600 (600/150 MHz) spectrometer. A LCQ liquid chromatrography mass spectrometry system and a Finnigan LTQ Orbitrap system were used for high-resolution mass spectrometry and protein conjugation analysis. Fourier transform infrared spectroscopy was performed on a Perkin-Elmer (Shelton, CT) Paragon 1000 FTIR spectrometer. Melting points were obtained using a SMP3 scientific melting apparatus (Stuart, Bibby Sterlin Ltd.)

Syntheses. *1,7-Di-Boc-1,4,7,10-tetraazacyclododecane-4,10-dimethyl Acetate (**1**).* BocOSu (2.49 g, 11.6 mmol) was dissolved in dry $CHCl_3$ (20 mL) and was added under argon to a cyclen (1 g, 5.8 mmol) solution in $CHCl_3$ (40 mL). The reaction mixture was stirred at room temperature for 36 h. To the reaction mixture 3 M NaOH (30 mL) was added and stirring was continued for 30 min. Brine (30 mL) was added and the solution was extracted with dichloromethane (3 × 20 mL). The organic fractions were combined, dried over $MgSO_4$ and concentrated *in vacuo*. The remaining colorless oil was dissolved in acetonitrile (30 mL). K_2CO_3 (1.94 g, 14.5 mmol) and methyl 2-bromoacetate (2.22 g, 14.5 mmol) were added into the solution and stirred for 12 h at room temperature. The reaction mixture was concentrated, dissolved in ethyl acetate and washed with brine. The organic layer was dried ($MgSO_4$), filtered and concentrated. The resulting residue was purified by column chromatograghy to yield compound **1** as a white amorphous solid (2.48 g, 83% yield), mp = 82−83 °C, R_f = 0.3 (5% MeOH in DCM). ^{1}H NMR (400 MHz $CDCl_3$): δ = 1.27 (s, 18H), 2.69 (br, 8H), 3.21 (br, 8H), 3.28 (s, 4H), 3.51 (s, 6H). ^{13}C NMR (100 MHz $CDCl_3$): δ = 28.14, 46.21, 50.98, 54.36, 54.54, 79.05, 155.51, 171.39. FTIR: 2975.8, 1739.6, 1683.9, 1364.7, 1157.3 cm^{-1}. HR-MS: *m*/*z* 517.3225 $[M+H]^+$, calcd $[C_{24}H_{45}N_4O_8]$ 517.3232.

*1,7-Dimethlyene-(p-nitrophenol)-1,4,7,10-tetraazacyclododecane-4,10-diacetic Acid (**3**).* Compound **1** (400 mg, 0.75 mmol) was dissolved in a mixture of dichloromethane and TFA (4 mL, 1:3 v/v) and stirred for 4 h at room temperature. The reaction mixture was concentrated under reduced pressure and coevaporated with toluene to remove the TFA. The crude mixture was dissolved in acetonitrile (10 mL). 2-Hydroxy-5-nitrobenzyl bromide (435 mg, 1.88 mmol) and K_2CO_3 (260 mg, 1.88 mmol) were added into the solution, which was stirred for 12 h at 80 °C. The reaction mixture was filtered and the solid was washed with acetonitrile (30 mL). The filtrate was concentrated *in vacuo* to give a yellow oil. The crude compound was dissolved in a solution mixture which contained 1,4-dioxane (final concentration was 15 mM) and 3 M NaOH (final concentration was 0.4 M). The solution was stirred at room temperature for 4 h, then concentrated under reduced pressure and purified by HPLC (0.1% TFA and a 10−50% acetonitrile gradient on C18 preparative column). ^{1}H NMR (400 MHz CD_3OD): δ = 3.19 (s, 8H), 3.33 (s, 4H), 3.44 (s, 8H), 4.64 (s, 4H), 7.12 (d, 2H), 8.30 (d, 2H), 8.54 (s, 2H). ^{13}C NMR (100 MHz CD_3OD): δ = 174.71, 164.29, 142.31, 130.87, 129.33, 117.59, 117.39, 54.15, 51.57, 49.87. FTIR: 3084.3, 1728.1, 1667.9, 1593.1, 1496.0, 1338.9, 1286.1, 1185.8, 1133.0, 1084.8 cm^{-1}. HR-MS: *m*/*z* 591.2409 $[M+H]^+$, calcd $[C_{26}H_{35}N_6O_{10}]$ 591.2409.

CLaNP-7. Compound **3** (296 mg, 0.5 mmol) was dissolved in DMF (10 mL) and treated with 2-(aminoethyl)methanethiosulfonate hydrobromide (283.4 mg, 1.2 mmol), NHS (345.3 mg, 3 mmol), and EDC (574.5 mg, 3 mmol). The reaction mixture was stirred overnight at room temperature. The reaction mixture was concentrated under reduced pressure and purified by HPLC (0.1% TFA and a 20−45% acetonitrile gradient on C18 preparative column) yielding CLaNP-7 (40%) as a yellow oil. ^{1}H NMR (600 MHz, DMSO-d^6, 323 K): δ = 3.09 (s, 8H), 3.21 (s, 4H), 3.27 (s, 8H), 3.31 (t, 4H), 3.47−3.53 (br, m, 10H), 7.12 (d, 2H), 8.21 (q, 2H), 8.47 (s, 2H), 8.51 (s, 2H). ^{13}C NMR (150 MHz, DMSO-d^6, 323 K): δ = 34.87, 38.21, 48.68, 49.80, 50.17, 51.52, 53.92, 116.40, 127.11, 129.22, 139.12, 164.06, 169.98. FTIR: 3465.8, 1649.8, 1138.9, 1198.9, 1134.5, 1100.8 cm^{-1}. HR-MS: *m*/*z* 865.2358 $[M+H]^+$, calcd $[C_{32}H_{49}N_8O_{12}S_4]$ 865.2347.

Lu-CLaNP-7. $Lu(OAc)_3$ (2.37 mg, 5.38 μmol) and CLaNP-7 (4.19 mg, 4.84 μmol) were separately dissolved in DMF (50 μL). Then, the CLaNP-7 solution was added into $Lu(OAc)_3$ solution and stirred for 4 h at room temperature. Without further purification, Lu-CLaNP-7 was

dx.doi.org/10.1021/ja307824e | J. Am. Chem. Soc. 2012, 134, 17306−17313

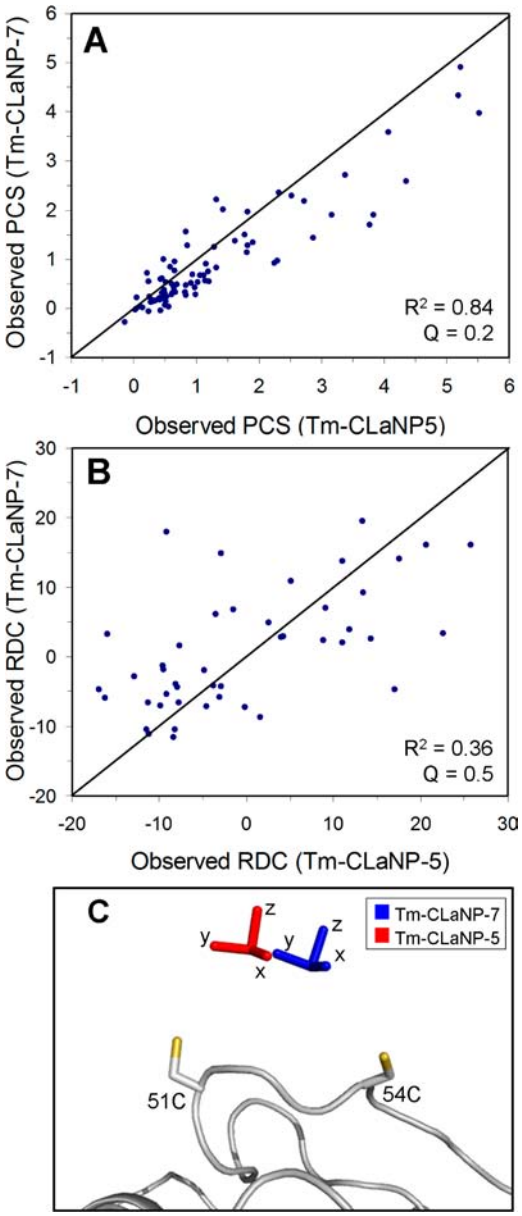

Figure 9. Comparison of CLaNP-5 and CLaNP-7. Experimentally observed PCSs and RDCs from Tm-CLaNP-7 plotted against the experimentally observed PCSs (A, $Q = 0.2$) and RDCs (B, $Q = 0.5$) from Tm-CLaNP-5 for Paz E51C/E54C. The solid line represents a perfect correlation. (C) Experimentally determined position and orientation of the Tm $\Delta\chi$-tensor relative to the Paz (PDB entry 1PY0)[32] structure for CLaNP-5 (red sticks) and for CLaNP-7 (blue sticks). The Cys side chains are shown in CPK colors.

used to label protein samples. The other lanthanide ions Yb, and Tm were chelated to CLaNP-7 following the same procedure. HR-MS: m/z 1036.1513 $[M-2H]^+$, calcd $[C_{32}H_{46}N_8O_{12}S_4Lu]$ 1037.1520.

Protein Production and Purification. The production and purification of the ^{15}N enriched *Alcaligenes faecalis* pseudoazurin (Paz) double cysteine mutant E51C/E54C was performed as described before,[32] with small modifications. Instead of *Escherichia coli* BL21 (DE3), *E. coli* BL21 (PlysS) was used to produce Paz E51C/E54C and Tris-HCl buffer (20 mM Tris-HCl, pH 7.0) was used for ion exchange chromotagraphy on the CM column. Double cysteine mutations I34C/V36C were prepared by the QuikChange method using the expression plasmid of wt Paz as a template.[42] The oligonucleotides 5′-GGCGACACGGTCACCTTTTGTCCGTGCGACAAAGGACA-TAATG-3′ and its complement were used as the forward and reverse primers, respectively. The expression and purification of the ^{15}N enriched variant was performed using the same conditions as described above. The final yield obtained for Paz I34C/V36C was 2.4 mg/L of culture. ^{15}N enriched yeast Cyt *c* N56C/L58C was produced and purified by the published method.[33] To create mutant Cyt *c* H39A/N56C/L58C, the forward and backward primers 5′-CTTGCATGG-TATCTTTGGCAGAGCCTCTGGTCAAGCTGAAGGGTATTCG-3′ and its complement were used on the template encoding Cyt *c* N56C/L58C. Expression and purification was identical to that of N56C/L58C. The final yield was 2.8 mg/L of culture.

Paramagnetic Probe Attachment. To attach Ln-CLaNP7 to Paz and Cyt *c*, protein sample (1 mL, 150−300 μM) was treated with DTT (final concentration 5 mM) at 0 °C for 1 h to remove possible dimers. The reaction mixture was loaded on a PD-10 column (GE Healthcare) pre-equilibrated with labeling buffer (20 mM sodium phosphate, 150 mM NaCl, pH 7.0) to remove DTT. To avoid any reoxidation by air, the buffer was degassed and the PD-10 column kept under an argon atmosphere. To the eluted protein five equivalents Ln-CLaNP-7 were added. The solution was stirred overnight at 4 °C. The probe attached Paz sample was concentrated to 500 μL and purified over a Superdex 75 gel filtration column. In the case of Cyt *c*, the protein was purified on a HiTrap-SP column. The yield of labeling, estimated from the intensity of diamagnetic peaks in the $[^{15}N,^1H]$-HSQC spectra of samples with paramagnetic tags, was more than 90%.

NMR Spectroscopy. The NMR samples of Paz Ln-CLaNP-7 (100−200 μM) were prepared in 20 mM sodium phosphate, 150 mM NaCl buffer, and 6% (v/v) D_2O. All Cyt *c* samples (100−200 μM) contained 20 mM sodium phosphate buffer, 6% (v/v) D_2O and 1 equiv of ascorbic acid under an argon atmosphere to keep the Cyt *c* in the reduced state. The pH of these samples was set with small aliquots of 0.1 M HCl or 0.1 M NaOH and was checked before each titration point. All $[^{15}N,^1H]$-HSQC and IPAP spectra[43] were recorded at 298 K on a Bruker Avance III 600 MHz spectrometer. Data were processed with NMRPipe[44] and analyzed with CCPNMR Analysis version 2.1.[45] Assignments of the resonances were based on previous work.[32,46,47]

PCS and RDC Analysis. PCS were defined as the chemical shift difference for a resonance in the paramagnetic and diamagnetic sample. Positioning of the metal and optimization of the $\Delta\chi$-tensor were preformed as described for CLaNP-5,[25] by using XPLOR-NIH version 2.9.9[48] and Pararestraints.[49] The structures of Paz and Cyt *c* were taken from PDB entries 1PY0 and 1YCC and hydrogens were added.[32,39] The variation in the Ln positions were calculated by randomly removing 20% PCS data and repeating the $\Delta\chi$-tensor fit 100 times. For RDC analysis, the HN positions were optimized on the basis of the experimental RDCs. The optimized structure was used for back-calculation of the RDCs on the basis of the PCS-derived $\Delta\chi$-tensor. The *Q* factor provides a normalized measure for the agreement between a set of observed and calculated experiment data:[50]

$$Q = \sqrt{\sum_i (O_i^{obs} - O_i^{calc})^2 / \sum_i (O_i^{obs} + O_i^{calc})^2} \quad (2)$$

where O_i^{obs} and O_i^{calcd} are the observed and calculated PCSs or RDCs.

■ ASSOCIATED CONTENT

Ⓢ Supporting Information

$[^{15}N,^1H]$-HSQC spectra of CLaNP-7- or CLaNP-5-tagged Cyt *c*; experimentally observed PCSs plotted against the backcalculated PCSs for Cyt *c* and Paz; model of CLaNP-7 linked to Paz I34C/V36C mutant; details of PCSs and RDCs data. This material is available free of charge via the Internet at http://pubs.acs.org.

■ AUTHOR INFORMATION

Corresponding Author

m.ubbink@chem.leidenuniv.nl

Notes

The authors declare no competing financial interest.

■ ACKNOWLEDGMENTS

Financial support was received from the Netherlands Organisation for Scientific Research, grants 700.58.405 (P.H.J.K.), 700.10.407 (M.A.S.H.), and 700.58.441 (W.-M.L., M.T., and M.U.)

■ REFERENCES

(1) Bertini, I.; Luchinat, C.; Parigi, G.; Pierattelli, R. *ChemBioChem* **2005**, *6*, 1536−1549.
(2) Clore, G. M. *Protein Sci.* **2011**, *20*, 229−246.
(3) Keizers, P. H. J.; Ubbink, M. *Prog. NMR Spectrosc.* **2011**, *58*, 88−96.
(4) Otting, G. *Annu. Rev. Biophys.* **2010**, *39*, 387−405.
(5) Pintacuda, G.; John, M.; Su, X.-C.; Otting, G. *Acc. Chem. Res.* **2007**, *40*, 206−212.
(6) Su, Y.; Hu, F.; Hong, M. *J. Am. Chem. Soc.* **2012**, *134*, 8693−8702.
(7) Bernini, A.; Spiga, O.; Venditti, V.; Prischi, F.; Botta, M.; Croce, G.; Tong, A. P.-L.; Wong, W.-T.; Niccolai, N. *J. Inorg. Biochem.* **2012**, *112*, 25−31.
(8) Kobashigawa, Y.; Saio, T.; Ushio, M.; Sekiguchi, M.; Yokochi, M.; Ogura, K.; Inagaki, F. *J. Biomol. NMR* **2012**, *53*, 53−63.
(9) Otting, G. *J. Biomol. NMR* **2008**, *42*, 1−9.
(10) Bertini, I.; Gupta, Y. K.; Luchinat, C.; Parigi, G.; Peana, M.; Sgheri, L.; Yuan, J. *J. Am. Chem. Soc.* **2007**, *129*, 12786−12794.
(11) Biekofsky, R. R.; Muskett, F. W.; Schmidt, J. M.; Martin, S. R.; Browne, J. P.; Bayley, P. M.; Feeney, J. *FEBS Lett.* **1999**, *460*, 519−526.
(12) Gay, G. L.; Lindhout, D. A.; Sykes, B. D. *Protein Sci.* **2004**, *13*, 640−651.
(13) Barthelmes, K.; Reynolds, A. M.; Peisach, E.; Jonker, H. R. A.; DeNunzio, N. J.; Allen, K. N.; Imperiali, B.; Schwalbe, H. *J. Am. Chem. Soc.* **2011**, *133*, 808−819.
(14) Gaponenko, V.; Dvoretsky, A.; Walsby, C.; Hoffman, B. M.; Rosevear, P. R. *Biochemistry* **2000**, *39*, 15217−15224.
(15) Ma, C.; Opella, S. J. *J. Magn. Reson.* **2000**, *146*, 381−384.
(16) Barb, A. W.; Ho, T. G.; Flanagan-Steet, H.; Prestegard, J. H. *Protein Sci.* **2012**, *21*, 1456−1466.
(17) Saio, T.; Ogura, K.; Shimizu, K.; Yokochi, M.; Burke, T.; Inagaki, F. *J. Biomol. NMR* **2011**, *51*, 395−408.
(18) Swarbrick, J. D.; Ung, P.; Su, X.-C.; Maleckis, A.; Chhabra, S.; Huber, T.; Otting, G.; Graham, B. *Chem. Commun.* **2011**, *47*, 7368−7370.
(19) Hallussinger, D.; Huang, J.-r.; Grzesiek, S. *J. Am. Chem. Soc.* **2009**, *131*, 14761−14767.
(20) Aime, S.; Botta, M.; Ermondi, G. *Inorg. Chem.* **1992**, *31*, 4291−4299.
(21) Aime, S.; Botta, M.; Fasano, M.; Marques, M. P. M.; Geraldes, C. F. G. C.; Pubanz, D.; Merbach, A. E. *Inorg. Chem.* **1997**, *36*, 2059−2068.
(22) Cosentino, U.; Villa, A.; Pitea, D.; Moro, G.; Barone, V.; Maiocchi, A. *J. Am. Chem. Soc.* **2002**, *124*, 4901−4909.
(23) Ranganathan, R. S.; Raju, N.; Fan, H.; Zhang, X.; Tweedle, M. F.; Desreux, J. F.; Jacques, V. *Inorg. Chem.* **2002**, *41*, 6856−6866.
(24) Keizers, P. H. J.; Desreux, J. F.; Overhand, M.; Ubbink, M. *J. Am. Chem. Soc.* **2007**, *129*, 9292−9293.
(25) Keizers, P. H. J.; Saragliadis, A.; Hiruma, Y.; Overhand, M.; Ubbink, M. *J. Am. Chem. Soc.* **2008**, *130*, 14802−14812.
(26) Vlasie, M. D.; Comuzzi, C.; van den Nieuwendijk, A. M. C. H.; Prudêncio, M.; Overhand, M.; Ubbink, M. *Chem.—Eur. J.* **2007**, *13*, 1715−1723.
(27) Polášek, M.; Kotek, J.; Hermann, P.; Císařová, I.; Binnemans, K.; Lukeš, I. *Inorg. Chem.* **2009**, *48*, 466−475..
(28) Woods, M.; Kiefer, G. E.; Bott, S.; Castillo-Muzquiz, A.; Eshelbrenner, C.; Michaudet, L.; McMillan, K.; Mudigunda, S. D. K.; Ogrin, D.; Tircsó, G.; Zhang, S.; Zhao, P.; Sherry, A. D. *J. Am. Chem. Soc.* **2004**, *126*, 9248−9256.
(29) De León-Rodríguez, L. M.; Kovacs, Z.; Esqueda-Oliva, A. C.; Miranda-Olvera, A. D. *Tetrahedron Lett.* **2006**, *47*, 6937−6940.
(30) Dapporto, P.; Fusi, V.; Micheloni, M.; Palma, P.; Paoli, P.; Pontellini, R. *Inorg. Chim. Acta* **1998**, *275*−*276*, 168−174.
(31) Li, C.; Winnard, P., Jr; Bhujwalla, Z. M. *Tetrahedron Lett.* **2009**, *50*, 2929−2931.
(32) Prudêncio, M.; Rohovec, J.; Peters, J. A.; Tocheva, E.; Boulanger, M. J.; Murphy, M. E. P.; Hupkes, H.-J.; Kosters, W.; Impagliazzo, A.; Ubbink, M. *Chem.—Eur. J.* **2004**, *10*, 3252−3260.
(33) Xu, X.; Keizers, P. H. J.; Reinle, W.; Hannemann, F.; Bernhardt, R.; Ubbink, M. *J. Biomol. NMR* **2009**, *43*, 247−254.
(34) Ni, W.; Fang, H.; Springsteen, G.; Wang, B. *J. Org. Chem.* **2004**, *69*, 1999−2007.
(35) Polášek, M.; Šedinová, M.; Kotek, J.; Vander Elst, L.; Muller, R. N.; Hermann, P.; Lukeš, I. *Inorg. Chem.* **2009**, *48*, 455−465..
(36) Green, K. N.; Viswanathan, S.; Rojas-Quijano, F. A.; Kovacs, Z.; Sherry, A. D. *Inorg. Chem.* **2011**, *50*, 1648−1655.
(37) Parker, D.; Puschmann, H.; Batsanov, A. S.; Senanayake, K. *Inorg. Chem.* **2003**, *42*, 8646−8651.
(38) Zhang, S.; Jiang, X.; Sherry, A. D. *Helv. Chim. Acta* **2005**, *88*, 923−935.
(39) Louie, G. V.; Brayer, G. D. *J. Mol. Biol.* **1990**, *214*, 527−555.
(40) Aime, S.; Barge, A.; Botta, M.; Fasano, M.; Danilo Ayala, J.; Bombieri, G. *Inorg. Chim. Acta* **1996**, *246*, 423−429.
(41) Jacques, V.; Desreux, J. F. *Inorg. Chem.* **1994**, *33*, 4048−4053.
(42) Ho, S. N.; Hunt, H. D.; Horton, R. M.; Pullen, J. K.; Pease, L. R. *Gene* **1989**, *77*, 51−59.
(43) Tjandra, N.; Omichinski, J. G.; Gronenborn, A. M.; Clore, G. M.; Bax, A. *Nat. Struct. Mol. Biol.* **1997**, *4*, 732−738.
(44) Delaglio, F.; Grzesiek, S.; Vuister, G. W.; Zhu, G.; Pfeifer, J.; Bax, A. *J. Biomol. NMR* **1995**, *6*, 277−293.
(45) Vranken, W. F.; Boucher, W.; Stevens, T. J.; Fogh, R. H.; Pajon, A.; Llinas, M.; Ulrich, E. L.; Markley, J. L.; Ionides, J.; Laue, E. D. *Proteins* **2005**, *59*, 687−696.
(46) Xu, X.; Reinle, W.; Hannemann, F.; Konarev, P. V.; Svergun, D. I.; Bernhardt, R.; Ubbink, M. *J. Am. Chem. Soc.* **2008**, *130*, 6395−6403.
(47) Worrall, J. A. R.; Kolczak, U.; Canters, G. W.; Ubbink, M. *Biochemistry* **2001**, *40*, 7069−7076.
(48) Schwieters, C. D.; Kuszewski, J. J.; Tjandra, N.; Clore, M. G. *J. Magn. Reson.* **2003**, *160*, 65−73.
(49) Banci, L.; Bertini, I.; Cavallaro, G.; Giachetti, A.; Luchinat, C.; Parigi, G. *J. Biomol. NMR* **2004**, *28*, 249−261.
(50) Bashir, Q.; Volkov, A. N.; Ullmann, G. M.; Ubbink, M. *J. Am. Chem. Soc.* **2010**, *132*, 241−247.